ON THE DEVELOPMENT OF AN OPTICAL RUBIDIUM VECTOR ATOMIC MAGNETOMETER

James A. McKelvy[1], *Irina Novikova*[2], *Eugeniy E. Mikhailov*[2], *Mario A. Maldonado*[2]
Isaac Fan[3], *Yang Li*[3], *Ying-Ju Wang*[3], *John Kitching*[3], *Andrey Matsko*[1]

[1]Jet Propulsion Laboratory, California Institute of Technology, Pasadena, CA 91109, USA
[2]Physics Department, College of William & Mary, Willaimsburg, VA 23187, USA
[3]National Institute of Standards and Technology, Boulder, CO 80305, USA
E-mail: james.a.mckelvy@jpl.nasa.gov

IGARSS 2023 - 2023 IEEE International Geoscience and Remote Sensing Symposium | 979-8-3503-2010-7/23/$31.00 ©2023 IEEE | DOI: 10.1109/IGARSS52108.2023.10283082

ABSTRACT

The precise measurement of magnetic fields is a fundamental tool of remote sensing. However, accurately measuring the direction of magnetic fields is challenging with atomic magnetometers. In this work, we discuss progress on the development of an all-optical vector atomic magnetometer that uses electromagnetically induced transparency (EIT) on ^{87}Rb vapor. The magnitude of the magnetic field is evaluated by measuring the separation of the laser transmission peaks of the Zeeman-resolved EIT spectra, and the direction is measured by evaluating the relative peak contrast using a lightweight machine learning algorithm involving principal component analysis (PCA). We have demonstrated a scalar sensitivity of $< 10pT/\sqrt{Hz}$ in the $1-100$ Hz band and an angular accuracy of $< 1°$. This approach for vector magnetometry does not require an array of sensors or calibration coils, ultimately setting the groundwork for the design of a new magnetometer that is lighter and more accurate than conventional vector magnetometer configurations.

Index Terms— Vector Magnetometry, Electromagnetically Induced Transparency, Principal Component Analysis

1. BACKGROUND

Optical vector atomic magnetometry is a maturing research area that is utilizing fundamental physics to create magnetic field sensors capable of performing both vector and scalar magnetic field measurements with high stability and accuracy. Magnetometers have historically been an enabling technology with a wide variety of applications, including geophysical surveys [1], planetary science [2, 3, 4], and unexploded ordnance detection [5]. However, despite the inherent vector properties of magnetic fields, many state of the art magnetometers are designed as scalar sensors and then retroactively configured to enable vector measurements [6, 7]. This phenomenon is particularly challenging for atomic magnetometers, which are generally designed to make precision measurements of the energy shifts of magneto-sensitive Zeeman sublevels of the ground state of alkali atoms. Under this design approach, these sensors are made to be highly sensitive to changes in the absolute local magnetic field, but impervious to changes in its direction.

Vector measurements can be performed by taking a scalar magnetometer and applying low frequency magnetic fields along a set of coordinate axes, but such methods require physically aligning the sensor's coordinate system into orthogonality [7, 8, 9]. With this technique, any mechanical misalignment will be directly translated into angular measurement error. Furthermore, these methods require adding magnetic coils to the system that introduce complex disturbances into the ambient magnetic field, possibly contaminating the signal of interest. As a result, the sensitivity of the vector device degrades significantly when compared with the scalar system based on the same principles [10, 11]. These challenges can be subverted with all-optical interrogation techniques that incorporate electromagnetically induced transparency (EIT), which provide a means to perform vector magnetic field measurements without the need for external calibration and complex magnetic coil systems [12]. In what follows, we discuss advancements in the design of an atomic magnetometer that utilizes EIT spectroscopy on ^{87}Rb vapor to create precision vector measurements of magnetic fields with an atomic basis.

A portion of this research was conducted at the Jet Propulsion Laboratory, California Institute of Technology, under contract with the National Aeronautics and Space Administration and funded by DARPA contract (81-110107). The views, opinions and/or findings expressed are those of the authors and should not be interpreted as representing the official views or policies of the Department of Defense or the U.S. Government.

2. METHODOLOGY

EIT is a two-photon transmission resonance caused by atoms prepared in a non-interacting quantum superposition of ground state sublevels. This is usually accomplished by tuning a bi-chromatic coherent light to interact with a quantum system in either a Λ or a more complex configuration [12]. If the light has high enough intensity, the fields establish the quantum coherence and create a narrow transparency resonance when two laser components are in two-photon Raman resonance with two of the atomic sublevels. Depending on the polarization of light and the number of available Zeeman sublevels, multiple Λ links and EIT resonances are formed. For example, for the ^{87}Rb D_1 line interrogated with $\mathrm{lin}||\mathrm{lin}$ polarized light, up to seven EIT peaks can be observed in the transmission spectrum when a magnetic field is present. Measurements of the separation frequency between these transmission peaks enables scalar measurements of the absolute magnetic field. Changes in the directionality of the magnetic field cause variations of the coupling strengths between the different Zeeman sublevels and the optical waves, which in turn results in variations of the contrast of the transmission peaks. These variations allow determination of the direction of the magnetic field vector with respect of the laser wave (**k**) vector and the direction of the input polarization of light. This approach forms a robust intrinsic coordinate system, as illustrated by with Fig.1. The idea was validated experimentally experimentally [12, 13].

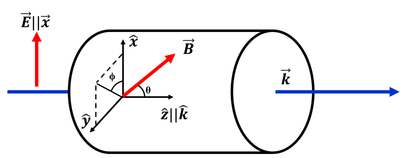

Fig. 1. Angle definitions for azimuthal angle ϕ and longitudinal angle θ with respect to laser **k** vector and polarization of light.

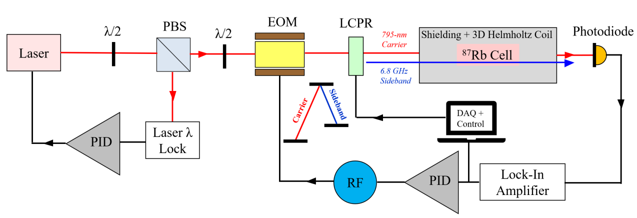

Fig. 2. Block diagram of the experimental setup for the EIT magnetometer.

A block diagram of the experimental setup for the magnetometer prototype is shown in Fig.2. A 795-nm laser is locked to the $5S_{1/2}F = 2 \rightarrow 5P_{1/2}F = 1$ resonance of ^{87}Rb using a reference Rb vapor cell, and then phase-modulated using an electro-optical modulator (EOM) and a 6.8 GHz RF source. The resulting polychromatic coherent light passes through a programmable liquid crystal polarization rotator (LCPR), and then propagates through a $100mm^3$ ^{87}Rb vapor cell inside of a magnetic shielding assembly. This shielding is needed for accurate measurement of device performance, and would not be required in a fieldable device. On the opposite side of the shield assembly, a photodiode and lock-in amplifier are used to record the light passing through the vapor cell. The 6.8 GHz source is swept over a 3 MHz range to observe all seven EIT resonances. Inside of the shield assembly, three pairs of orthogonal Helmholtz coils are used to generate a magnetic field with an arbitrary direction.

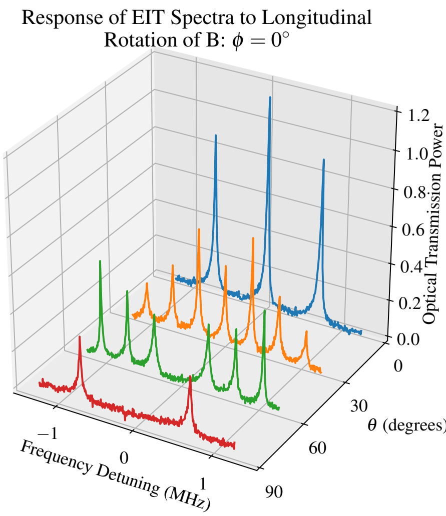

Fig. 3. EIT spectra observed with experimental setup.

2.1. Scalar Sensitivity

Examples of the EIT spectra observed for various values of θ are shown in Fig.3. Since the γ-factor for Rb two ground-state hyperfine levels are similar, the EIT peaks occur at the detunings from the unshifted hyperfine splitting by integer multiple m of the Zeeman shift. While variations in the direction of the field change the contrast of the EIT spectra, two of the EIT resonances occur for all possible values of ϕ and θ (the $m_{\pm 2}$ resonances). Precision measurements of the magnitude of the local magnetic field are collected by modulating the probe frequency to hop between the $m_{\pm 2}$ resonances and recording the frequency separation between them. An example of the magnetic sensitivity produced with this methodology is shown in Fig.4. For this measurement, the Helmholtz coils were used to maintain a fixed magnitude of B at 50 μT (the nominal magnitude of Earth's field). The low noise performance has been achieved by careful optimization of the temperature of the ^{87}Rb vapor cell and the RF power driving the EOM. At the time of writing, the achievable stability of this configuration is limited by the stability of the current source powering the Helmholtz coils. However, the theoretical sensitivity limit of the device is estimated to be $1pT/\sqrt{Hz}$. This result is not competitive with Spin-Exchange Relaxation Free (SERF) magnetometers, which have demonstrated magnetic sensitivity $< 0.2fT/\sqrt{Hz}$ [14]. However, the scalar sensitivity of the Rb EIT magnetometer is comparable to that of the fluxgate magnetometer [15], but with the added benefit of angular sensitivity and accuracy made possible within a single sensor. Fluxgate magnetometers and similar sensors can be configured to make vector measurements as well; however, these methods require an array of sensors to be arranged on orthogonal axes to measure all components of the magnetic field.

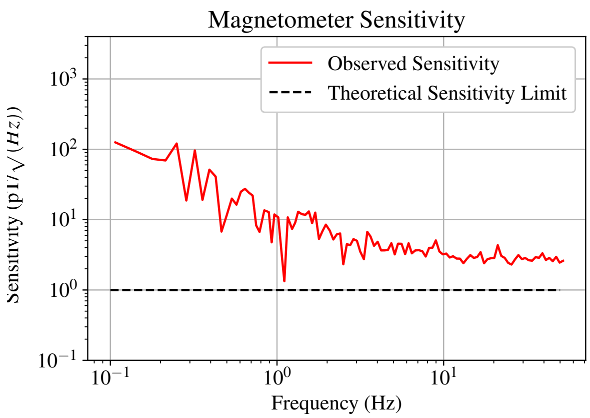

Fig. 4. Scalar magnetic sensitivity observed with the Rb EIT magnetometer at 50 μT.

2.2. Angular Sensitivity

The optimal method for processing observations of the EIT spectrum for vector measurements was developed using unsupervised machine learning techniques, with principal component analysis (PCA) ultimately selected as the optimal method of angle determination [16]. This method uses a library of EIT spectra to calculate a new orthonormal basis that maximizes the variance of the EIT data set. Particular manifestations of the EIT spectra can be projected onto this basis, which allows high dimensional spectrum measurements to be represented in a reduced dimensional subspace. Projections of the EIT spectra onto this basis are then used as features to train a support vector regression (SVR) model that correlates different manifestations of the EIT spectra back to specific components of the observed magnetic field vector. Projections of the EIT spectra onto the first two principal axes of the EIT data set are shown in Fig.5.

A data set consisting of 1,400 observations of the EIT spectrum was collected to develop the PCA-SVR algorithm for recovering the longitudinal angle θ and magnitude B from EIT measurements. This data was collected by adjusting the

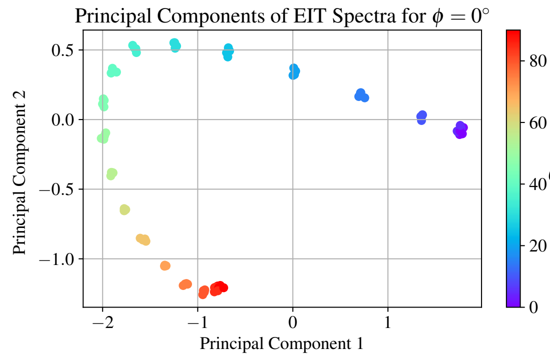

Fig. 5. Principal components of the EIT spectra. Note that the components of the spectra cluster at specific values of θ.

currents in the three dimensional Helhmholtz coil in the experimental setup to vary θ from $0-90°$ and B from 50-55 μT. Previous studies have demonstrated that the greatest angular sensitivity is achieved when the input polarization of light is locked to $\phi = 0°$ [16], and so the LCPR was controlled to maintain this setting throughout these measurements. Of the 1,400 observations, 1,000 samples were used to define the principal axes and train the SVR model (using five-fold cross validation). The overall performance of the technique was evaluated by projecting the remaining 400 samples onto the new principal axes and using the SVR model on the resulting projections to predict θ and B. The result of this analysis is shown in Fig.6, in which the error of each vector prediction is expressed in terms of the separation angle between the predicted vector and the true vector associated with that observation. The total standard deviation of the method was found to be approximately $0.83°$. While the PCA method initially shows decreased sensitivity for $\theta \leq 5°$, this limitation can be overcome with a two-stage measurement involving nonlinear extensions of PCA such as kernel principal component analysis [16].

3. CONCLUSION

We have created a breadboard prototype of the magnetometer using a $100mm^3$ atomic cell interrogated with micro-Watts of laser power. Scalar measurements have been demonstrated by evaluating the separation of the EIT resonances, and vector measurements are performed by processing the spectra with the PCA-SVR algorithm. The prototype EIT magnetometer has produced magnetic scalar sensitivity better than $10pT/\sqrt{Hz}$ in the 1-100Hz range, and angular accuracy better than $1°$. At least an order of magnitude improvement of the sensitivity is feasible, in accordance with our theoretical analysis. The proposed technology, when matured, will provide new capabilities for absolute magnetometry in remote sensing.

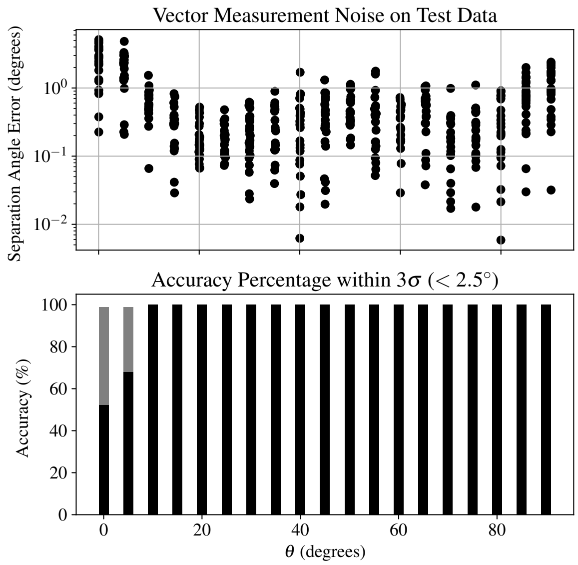

Fig. 6. Vector measurement error observed with the Rb EIT magnetometer. The accuracy metric refers to the percentage of predictions that fall within 3σ of the true value for each value of θ. The typical accuracy at $\theta = 0°$ is $\pm 3°$. Sensitivity better than $\pm 1°$ can be achieved with kernel PCA (expected improvement at small angles is shown by gray color) [16].

4. REFERENCES

[1] N. Olsen, G. Hulot, V. Lesur, and C. et al. Finlay, C. C.and Beggan, "The swarm initial field model for the 2014 geomagnetic field," *Geophysical Research Letters*, vol. 42, no. 4, pp. 1092–1098, 2015.

[2] K.-H. Glassmeier, H.-U. Auster, D. Heyner, K. Okrafka, and C. et al. Carr, "The fluxgate magnetometer of the bepicolombo mercury planetary orbiter," *Planetary and Space Science*, vol. 58, no. 1, pp. 287–299, 2010.

[3] J. E. P. Connerney, J. Espley, P. Lawton, S. Murphy, J. Odom, R. Oliversen, and D. Sheppard, "The maven magnetic field investigation," *Space Science Reviews*, vol. 195, no. 1, pp. 257–291, December 2015.

[4] J. T. Hoeksema, Y. Liu, K. Hayashi, X. Sun, and J. et al. Schou, "The helioseismic and magnetic imager (hmi) vector magnetic field pipeline: Overview and performance," *Solar Physics*, vol. 289, no. 9, pp. 3483–3530, September 2014.

[5] K. M. Churchill, C. Link, and C. C. Youmans, "A comparison of the finite-element method and analytical method for modeling unexploded ordnance using magnetometry," *IEEE Transactions on Geoscience and Remote Sensing*, vol. 50, no. 7, pp. 2720–2732, 2012.

[6] R. E. Slocum and F. N. Reilly, "Low field helium magnetometer for space applications," *IEEE Transactions on Nuclear Science*, vol. 10, no. 1, pp. 165–171, 1963.

[7] A. J. Fairweather and M. J. Usher, "A vector rubidium magnetometer," *Journal of Physics E: Scientific Instruments*, vol. 5, no. 10, pp. 986, oct 1972.

[8] W. F. Stuart, "Earth's field magnetometry," *Reports on Progress in Physics*, vol. 35, no. 2, pp. 803, may 1972.

[9] O. Gravrand, A. Khokhlov, J. L. Le Mouël, and J. M. Léger, "On the calibration of a vectorial ^{4}he pumped magnetometer," *Earth, Planets and Space*, vol. 53, no. 10, pp. 949–958, 2001.

[10] G. Hulot, P. Vigneron, J. M. Leger, I. Fratter, and N. et al. Olsen, "Swarm's absolute magnetometer experimental vector mode, an innovative capability for space magnetometry," *Geophysical Research Letters*, vol. 42, pp. 1352 – 1359, 2015.

[11] G. Hulot, J. M. Léger, P. Vigneron, T. Jager, and F. et al. Bertrand, "Nanosatellite high-precision magnetic missions enabled by advances in a stand-alone scalar/vector absolute magnetometer," in *IGARSS 2018 - 2018 IEEE International Geoscience and Remote Sensing Symposium*, 2018, pp. 6320–6323.

[12] V. I. Yudin, A. V. Taichenachev, Y. O. Dudin, V. L. Velichansky, A. S. Zibrov, and S. A. Zibrov, "Vector magnetometry based on electromagnetically induced transparency in linearly polarized light," *Phys. Rev. A*, vol. 82, pp. 033807, Sep 2010.

[13] K. Cox, V. I. Yudin, A. V. Taichenachev, I. Novikova, and E. E. Mikhailov, "Measurements of the magnetic field vector using multiple electromagnetically induced transparency resonances in rb vapor," *Phys. Rev. A*, vol. 83, pp. 015801, Jan 2011.

[14] H. B. Dang, A. C. Maloof, and M. V. Romalis, "Ultrahigh sensitivity magnetic field and magnetization measurements with an atomic magnetometer," *Applied Physics Letters*, vol. 97, no. 15, 10 2010, 151110.

[15] C. T. Russell, B. J. Anderson, W. Baumjohann, K. R. Bromund, and D. et al. Dearborn, "The magnetospheric multiscale magnetometers," *Space Science Reviews*, vol. 199, no. 1, pp. 189–256, 2016.

[16] J. A. McKelvy, I. Novikova, E. E. Mikhailov, M. Gonzalez, I. Fan, Y. Li, Y. J. Wang, J. Kitching, and A. Matsko, "Application of Kernel Principal Component Analysis for Optical Vector Atomic Magnetometry," *TechRxiv*, May 2023.